Optimising the 3-channel microfluidic system to investigate chemical gradient impacts on bacterial chemotaxis in fluid and near surfaces

Adam Gargasson, Julien Bouvard, Carine Douarche, Peter Mergaert, Harold Auradou

Optimising the 3-channel microfluidic system to investigate chemical gradient impacts on bacterial chemotaxis in fluid and near surfaces

Adam Gargasson[1], Julien Bouvard[1], Carine Douarche[1], Peter Mergaert[2], Harold Auradou[1]

[1]Université Paris-Saclay, CNRS, FAST, 91405 Orsay, France

[2]Université Paris-Saclay, CNRS, I2BC, 91190 Gif-sur-Yvette, France

Correspondence: harold.auradou@universite-paris-saclay.fr

November 12, 2025

Abstract

Bacteria can adjust their swimming behaviour in response to chemical variations, a phenomenon known as chemotaxis. This process is characterised by a drift velocity that depends non-linearly on the concentration of the chemical species and its local gradient. To study this process more effectively, we optimised a 3-channel microfluidic device designed to create a stable gradient of chemoattractants. This setup allows us to simultaneously monitor the response of *Escherichia coli* to casamino acids or α-methyl-DL-aspartic acid at the individual level.

1 Introduction

Chemotaxis is a phenomenon that allows bacteria to actively modulate their movement to move up or down chemical gradients. Bacteria are then able to detect and navigate towards nutrients while avoiding potential toxins or adverse conditions [1–3]. Chemotaxis is an essential phenomenon in many biological processes, including microbiome assembly [4], symbiotic interactions [5] such as plant root colonisation [6] or insect gut infection [7], as well as biofilm formation [8–11]. It also allows bacteria to move towards polluted areas of soil or sediments and is expected to contribute to the optimisation of soil bio-decontamination technologies [12–16].

Various methods are available to study bacterial chemotaxis systematically: capillary assays [17], densiometry assays [18, 19], stopped-flow diffusion chambers [20, 21], or swarm plate assays [22, 23]. These traditional methods are accessible and well-established; however, the chemical gradients they create are challenging to control and can change over time. The use of microfluidic technologies in microchip development addresses this challenge by enabling the creation of controlled environments on micro- to millimetre scales. Microfluidic chips also provide a mean to visualise bacteria using microscopy. This capability has facilitated the reconstruction of bacterial trajectories and the assessment of their mobility based on the given environment. This technology has advanced quickly, leading to the development of various systems that allow for the observation of microorganisms in different gradients [24–27].

One of these methods is based on the use of a three-channel microfluidic chip (see Fig. 1) [28–32], composed of three parallel channels between which chemical species can diffuse. A linear chemical gradient is established by flowing solutions at different concentrations in the two outermost channels. The bacteria are then placed in the central channel and observed by a microscope. If chemotaxis occurs, the bacteria will migrate along the gradient. Several setups using a 3-channel chip have been used to quantify the chemotactic or aerotactic behaviour of bacteria [25, 33, 34], particularly focusing on *E. coli* chemotaxis toward α-methyl-DL-aspartic acid (MeAsp) [30, 31, 35]. In these studies, chemotaxis was characterised by observing the stationary distribution of bacteria across the width of the central channel.

Generally, the dynamics of the bacterial density $b(\mathbf{r}, t)$ can be described by the convection-diffusion equations [36, 37]:

$$\frac{\partial b}{\partial t} + \boldsymbol{\nabla} \cdot \mathbf{J} = 0, \qquad \mathbf{J} = b\mathbf{v_c} - \mu(c)\boldsymbol{\nabla} b = b\mathbf{v}, \qquad (1)$$

with **J** the bacterial flux in number of bacteria crossing a surface per unit of time, and c the concentration of chemical attractant. The first contribution in **J** is the chemotactic flux, i.e. the bacterial flow caused by the inhomogeneity of the attractant distribution. The second contribution in Eq. (1) is the diffusive flux, with $\mu(c)$ the diffusion coefficient associated with random swimming. The net flux resulting from the two fluxes is $b\mathbf{v}$. In the stationary phase the chemotactic velocity is simply balanced by diffusion, resulting in a bacterial concentration profile decreasing exponentially. The chemotactic velocity v_c is then calculated using the characteristic length λ associated with the exponential decrease of the profile $b(y)$ as $v_c = \mu/\lambda$. A great amount of experimental and modelling effort has been directed at determining the dependence of the chemotactic velocity on the attractant concentration c. In the limit of shallow gradients (i.e. $v_c/v_s \ll 1$ where v_s is the swimming velocity) [37, 38] along the direction y, the chemotactic velocity v_c is proportional to the attractant gradient with

$$v_c = \chi(c)\partial c/\partial y, \tag{2}$$

where $\chi(c)$ represents the chemotactic coefficient, accounting for the non-linear dependence of the chemotactic velocity on the attractant concentration. [20, 21, 37, 39]. Recent studies revealed the complexity of the time scales associated with the cellular signalling pathway [40]. They showed the existence of an adaptation dynamics of the signal transduction pathway, mediated by the chemosensors' methylation, which is slow compared to the typical run time, revealing the need to include these dynamics in the coarse-grained models [41]. Thus, additional variables like the average methylation level of the receptors [30, 42, 43] need to be considered. When the stimulus variation is relatively small, the model gives

$$\chi(c) = \frac{\chi_0}{(1 + c/c_-)(1 + c/c_+)} \tag{3}$$

where c_- and c_+ are the binding affinities of the receptor at respectively low and high methylation level [43, 44]. For $c_- \ll c \ll c_+$, Eq. (3) gives $\chi(c) \propto 1/c$ or $v_c \propto \nabla c/c \sim \ln(\nabla c)$. Thus, when taking into account the slow dynamics of the signalling pathway, chemotaxis is log-sensing [30, 33]. However, this sensitivity is not always observed for aerotaxis [45]. For some bacteria such as *Shewanella oneidensis* and *Burkholderia contaminans*, $v_c \propto \nabla c/c^2$ is observed [46, 47].

The present study accomplishes two key objectives. First, it demonstrates the flexibility of the 3-channel method by overcoming time constraints, allowing measurements at any moment and in multiple positions within the central channel. Second, the study emphasizes how surfaces significantly influence bacterial chemotaxis, which has important implications for understanding this process in porous media. To achieve our goal, we conduct local measurements of bacterial trajectories to quantify the chemotactic velocity $v_c(c)$ and susceptibility $\chi(c)$ of the bacterium *E. coli* in response to various gradients of MeAsp and casamino acids. We then compare our findings with the values obtained from observing the long-term stationary distribution of the bacteria.

2 Materials and methods

2.1 Microorganism and Growth Conditions

E. coli strain RP437-YFP expressing yellow fluorescent protein was grown in a minimal salt medium (M9G), consisting of M9 minimal medium salts supplemented with 0.1 % casamino acids, 0.4 % glucose, 0.1 mM calcium chloride and 2 mM magnesium sulfate in milliQ water. To this growth medium, 25 µg/mL chloramphenicol (CAM) was added to select for the plasmid carrying the yellow fluorescent protein gene. The bacteria were cultured in an incubator shaker at 240 rpm and 30 °C. A preculture was grown to an OD close to 0.3 and washed twice by centrifugation (2300 g for 10 min). The bacteria were then re-suspended into a minimal motility buffer (MB; 0.1 M EDTA, 1 mM methionine, 1 M sodium lactate, and 0.1 M Phosphate buffer in milliQ water at pH = 7.0). This medium provides the salts needed for bacterial swimming, but without any nutrients to prevent bacterial growth. The final suspension concentration is initially adjusted to an optical density (OD) between 0.06 and 0.1.

2.2 Fabrication and assembly of the setup

The protocol follows the work of Gargasson *et al.* [35]. In brief, we utilize a microfluidic chip constructed with three parallel channels, each 600 µm wide, separated by walls that are 200 µm thick, and with a height of 120 µm (see Fig. 1). The chip is made from polydimethylsiloxane (PDMS), which allows oxygen to permeate, ensuring consistent bacterial motility throughout the experiments. This chip is positioned on a 1 mm thick layer of a 3 % agar-agar gel, which is placed on a glass slide. Chemical solutions and bacterial suspensions are drawn into the device at a rate of 10 µL/s using a syringe pump. Special care is taken during setup and installation to prevent air bubbles from entering the channels and tubes.

2.3 Chemotaxis experiment

The experiment begins by placing the drain and source inlet tubes in microtubes containing the chemoattractants at the concentrations to be tested. The flow rate is reduced to 1 µL/s. Once the fluids have reached the channels, the gradient between the channels is established within 30 min [35]. When the central channel is filled with bac-

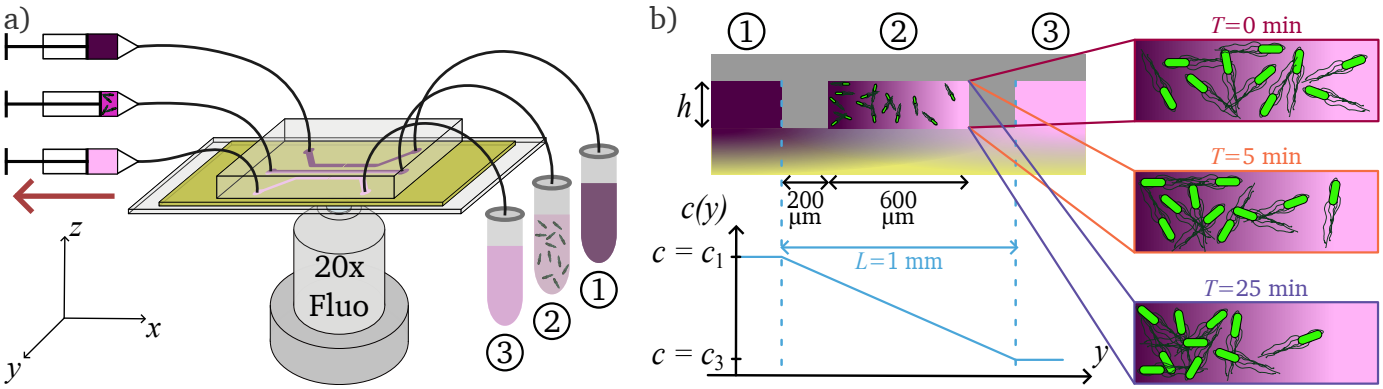

Figure 1: Sketch of the experimental setup. (a) The microfluidic chip, placed on an inverted microscope and observed under 20× magnification, consists of three parallel channels. The channels ① and ③ are filled with a chemo-attractant at concentration c_1 and c_3 diluted in the motility buffer (MB). (b) The chemo-attractant diffuses through the agarose layer, creating a linear gradient between channels ① and ③, notably in channel ② where fluorescent *E. coli* bacteria are injected. At $T = 0$, the bacteria are homogeneously distributed along the y-axis, before starting to accumulate towards the source of chemoattractant.

teria, the central channel pump is switched off, and the valve connecting the outlet to the microtube containing the bacterial suspension is closed to reduce any residual flux along the channel. The central channel is observed under fluorescence with a 20× objective. The field of view is 660 µm × 660 µm to allow for the imaging of the entire width of the channel, with a field depth of (37 ± 5) µm.

We used two attractants: casamino acids, obtained from MP Biomedicals LLC and α-methyl-DL-aspartic acid (MeAsp), obtained from MedChemExpress. Casamino acids are a mixture of amino acids and its molecular weight was taken to be approximately 100 g/mol, while α-methyl-DL-aspartic acid is $C_5H_9NO_4$ with a molecular weight of 147 g/mol. The average concentration is defined as $\bar{c} = (c_1 + c_3)/2$ and the gradient is $\nabla c = (c_1 - c_3)/L$. Some experiments are performed with $c_3 = 0$ mM; in this case, the value of $\nabla c/\bar{c} = 2/L$ is constant.

2.4 Data analysis of the bacteria trajectories

The experiments typically consist of recording films at seven times, spaced by 1–5 min, at the three different z positions: $z = 0$ (on the agar), $z = h/2$ (half-height in the bulk) and $z = h$ (on the PDMS). The time at which a sequence of three films is acquired is noted T. The measurement of T begins when the pump stops injecting bacteria into the central channel. Films were recorded at 10 frames per second at different times during the experiment. They lasted between 20 s and 60 s, consisting of 200–600 images. Bacterial tracks were computed from the sequences of phase fluorescent images using TrackMate [48], before being post-processed using an in-house Python code. Examples of tracks obtained are shown in Fig. 2. For each track i, the two-dimensional positions $\mathbf{x}_i(t) = (x_i(t), y_i(t))$ were measured, from which the two-dimensional velocities $\mathbf{v}_i(t) = \delta\mathbf{x}_i/\delta t$ using a sampling time $\delta t = 0.1$ s were computed. Only tracks longer than one second, which correspond to trajectories made over ten (x_i,y_i) positions, were retained. Additionally, to separate motile bacteria from non-motile bacteria, the average velocity, $\bar{v}_i$ of each track was calculated and tracks with $\bar{v}_i < 5$ µm/s were removed.

The chemotactic velocity is obtained from Eq. (1), which for a 1D gradient along y gives:

$$v_c(y,z,T) = v(y,z,T) + \frac{\mu}{b(y,z,T)}\frac{\partial b(y,z,T)}{\partial y} \qquad (4)$$

In this expression, μ is assumed to be constant and independent of the chemoattractant concentration. This assumption was experimentally verified (see SM A). We defined the diffusive velocity as

$$v_\mu(y,z,T) = -\frac{\mu}{b(y,z,T)}\frac{\partial b(y,z,T)}{\partial y} \qquad (5)$$

such that :

$$v_c(y,z,T) = v(y,z,T) - v_\mu(y,z,T). \qquad (6)$$

The dependency on height z is omitted for simplification, as the height will always be explicitly stated (either $z = 0$, $h/2$, or h). The spatial distribution of bacteria $b(y,T)$ and the diffusion coefficient μ are essential to calculate the chemotactic velocity, and, thus, the chemotactic response of *E. coli*.

To determine the profile $b(y,T)$, the data were spatially binned in the gradient direction over a band of width Δy, chosen as $\Delta y = 40$ µm because it is slightly longer than one correlation length of the bacterial trajectories ($l \sim v_s\tau \sim 25$ µm). The local gradient of $b(y,T)$ is calculated by determining the difference in the bacterial population

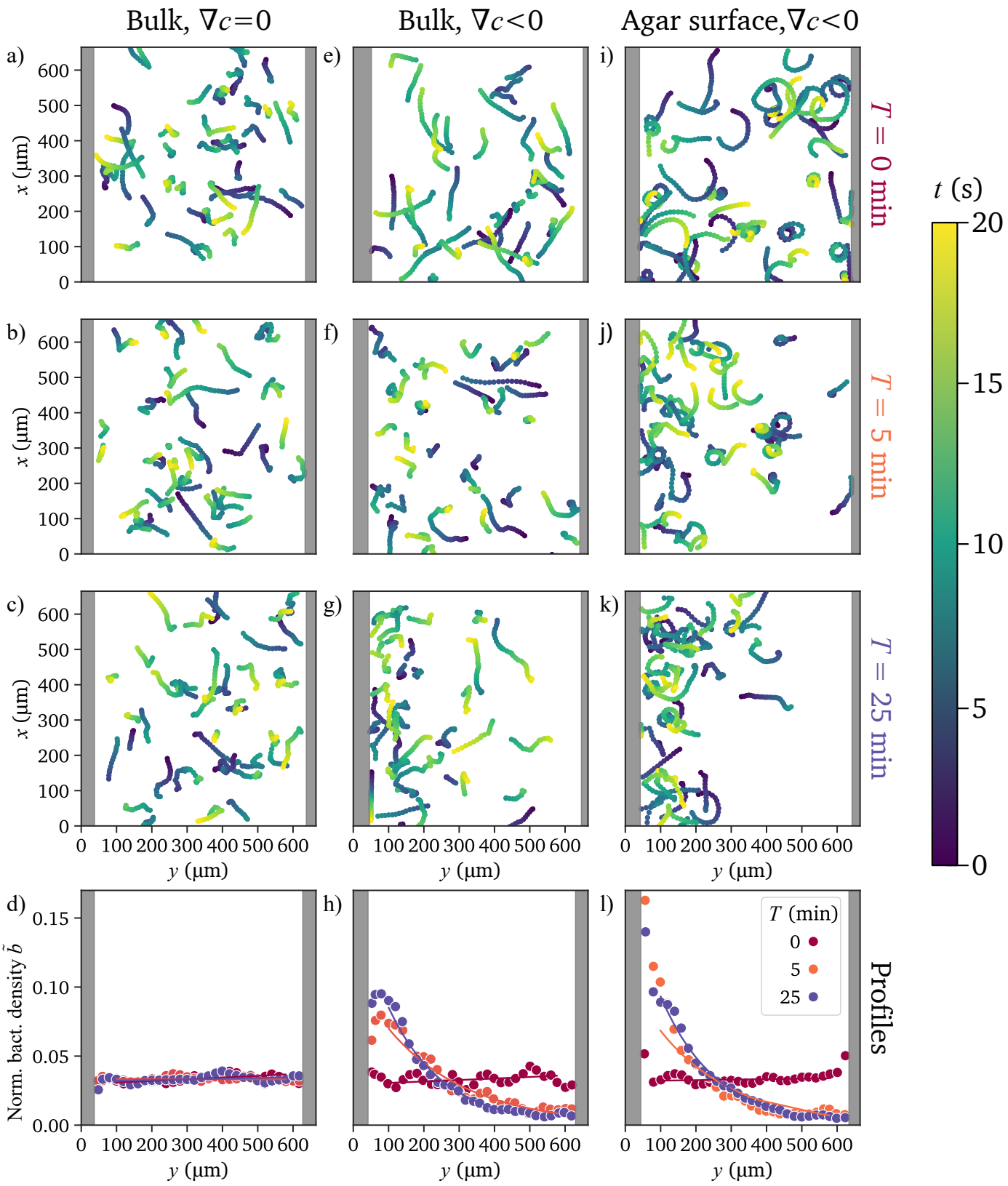

Figure 2: Bacterial tracks and concentration profiles for two experiments. Trajectories of *E. coli* bacteria are shown at three different times T during two experiments: without any gradient in the bulk $z = h/2$ (a-c), and with a 200 µM/mm MeAsp gradient either in the bulk $z = h/2$ (e-g) or on the bottom agar surface $z = 0$ (i-k). The tracks are colour-coded with the time t from 0–20 s. The corresponding bacterial profiles, measured at $T = 0$ min (●), 5 min (●) and 25 min(●), are displayed at the bottom of each column (d,h,l).

between the band below $b(y-\Delta y,T)$ and the one above $b(y+\Delta y,T)$ and dividing this difference by the distance between the two bands, which is $2\Delta y$.

The diffusion coefficient μ is given by $\mu = v_s^2\tau$ [49–51], where τ is the characteristic time of the exponential decrease of the velocity correlation functions, and v_s is the swimming velocity defined as $v_s = \langle|\mathbf{v}_i\cdot\mathbf{e}_y|\rangle_i$, $\langle\cdot\rangle_i$ representing the average calculated across all tracks in a particular film [35]. In SM A, we show the swimming velocity and correlation time values obtained for our experiments. Neither values seem to be influenced by chemoattractants. Practically, the values of the diffusion coefficient μ have been recalculated for each film. This has the advantage of accounting for changes in motility between batches of bacteria.

The diffusive velocity $v_\mu(y,T)$ is then given by:

$$v_\mu(y,T) = -\mu\frac{b(y+\Delta y,T)-b(y-\Delta y,T)}{2b(y,T)\Delta y}, \qquad (7)$$

and the net velocity by:

$$v(y,T) = \left\langle \mathbf{v}_i\cdot\mathbf{e}_y;\, y_i\in\left[y-\frac{\Delta y}{2},y+\frac{\Delta y}{2}\right]\right\rangle_{\Delta y}. \qquad (8)$$

In this equation, the brackets $\langle\cdot\rangle_{\Delta y}$ represent the average of all tracks whose positions fall within a band of width Δy that is centred at y. The Eqs (7)-(8) are applied to bands where the number of bacteria $b(y)$ is more than one-tenth of the maximum of $b(y)$. The chemotactic velocity $v_c(y,T)$ is obtained by summing the net $v(y,T)$ and diffusive $v_\mu(y,T)$ velocities. The velocities can be averaged over y to calculate the average chemotactic velocity $\bar{v}_c(T) = \langle v_c(y,T)\rangle_y$, the average diffusive velocity $\bar{v}_\mu = \langle v_\mu(y)\rangle_y$, and the average net velocity $\bar{v}(T) = \langle v(y,T)\rangle_y$. The average velocities normalised by the swimming velocity $v_s(T)$ are noted $\tilde{v}_c(T)$, $\tilde{v}_\mu(T)$ and $\tilde{v}(T)$. Finally, $\tilde{v}_c(T)$ can be divided by the average gradient, ∇c, defined in Sec. 2.3 to obtain $\chi(T)$ for a specific film. Note that the chemotactic susceptibility χ is calculated using the *normalised* chemotactic velocity, meaning its unit is $[\chi] = \mu\text{m}/\mu\text{M}$. This definition of χ allows for a more accurate comparison of bacterial batches with different v_s.

2.5 Detection threshold of chemotactic velocity

To assess the reliability of the setup, four control experiments were conducted without a gradient, meaning that the concentrations in both lateral channels were equal ($c_1 = c_3$). Three of these experiments had a concentration of $c_1 = c_3 = 0$, while one experiment used a concentration of $c_1 = c_3 = 42\,\text{mM}$ of casamino acids. The chemotactic velocity measured in these experiments was centred on $(0.1\pm0.7)\,\mu\text{m/s}$, confirming the absence of chemotaxis or the existence of fluid flows along y. The 95 % confidence interval, which indicates a chemotactic velocity lower than 5 % of the swimming velocity, reflects the precision of our experimental setup. Therefore, this threshold of $0.05\,v_s$ is selected as the point at which we can confidently assert that a significant chemotactic response occurs.

3 Results

The quantification of the chemotaxis of *E. coli* bacteria towards MeAsp and casamino acids is carried out in a microfluidic chip consisting of three parallel channels, following the protocol of [35] inspired by [25, 31], as depicted in Fig. 1. Figure 2 illustrates our observations after tracking the bacteria and reconstructing their trajectories from 20-second films. It presents two experiments conducted at different times, $T = 0\,\text{min}$, 5 min and 25 min, as well as different heights: films taken at mid-channel height (Fig. 2e-g) and on the agar surface (Fig. 2i-k). When there is no chemical gradient in the central channel, no evolution is observed in the bacterial trajectories, see Fig. 2a-c. The distribution of bacteria in the channel does not change over the course of an experiment; the population remains uniformly distributed in the canal at all times, as shown in Fig. 2d. The observed profiles are consistent with the trajectories shown in Fig. 2a-c which shows bacteria present throughout the canal with trajectories that move in all directions without any preferential direction.

When experiments are conducted using a gradient of chemoattractant, the concentration profiles of bacteria change over time. A significant accumulation of bacteria is observed on the side of the channel that is closest to the source with the highest concentration of chemoattractant. Trajectories of bacteria in a 200 µM/mm MeAsp gradient, recorded in the bulk $z = h/2$, are shown in Fig. 2e-g. This accumulation typically takes place over several minutes and reaches a stationary state characterized by an exponential concentration profile of bacteria, see Fig. 2h, as expected for such a linear gradient and as already reported in the literature [25, 30, 31, 33]. The characteristic length λ that is associated with the exponential decay of the profile $b(y)$ is then used to estimate the chemotactic velocity, v_c, using the relation $v_c = \mu/\lambda$. This method requires establishing a stationary profile, which may take several minutes to achieve. In Sec. 3.1, we will demonstrate that the chemotactic velocity can be measured from any film taken at any time by analysing the net and diffusive velocities computed from the bacteria trajectories. Following that, we will show in Sec. 3.2 how the method can be applied to determine a local chemotactic velocity. Furthermore, all our measurements will be used to construct the chemotactic susceptibility curve $\chi = f(c)$. Finally, we will study bacterial chemotaxis on surfaces in Sec. 3.3

by analysing movies recorded at different heights in the channel, $z = 0$, $z = h/2$ and $z = h$.

3.1 Chemotactic velocity

The method we propose for quantifying the chemotactic velocity of bacteria is based on calculating local bacterial fluxes derived from analysing their trajectories. The flux is decomposed into a convective and a diffusive part, and the chemotactic flux is obtained from a balance of the two. Conservation of fluxes allows us to obtain the chemotactic velocity as expressed by Eq. (6), which can be spatially averaged over y, yielding: $\bar{v}_c(T) = \bar{v}(T) - \bar{v}_\mu(T)$. After normalisation by the swimming velocity, we obtain $\tilde{v}_c(T) = \tilde{v}(T) - \tilde{v}_\mu(T)$. Evaluating the diffusive flux $\mu(c)\partial b/\partial y$ accurately can turn out to be quite delicate [47], as the bacteria motility might depend on the local concentration c or the concentration experienced during a specific duration. However, the weak dependence of the bacteria diffusivity μ on the chemoattractants' concentration used in this study circumvents this issue and allows us to do it consistently (see SM A).

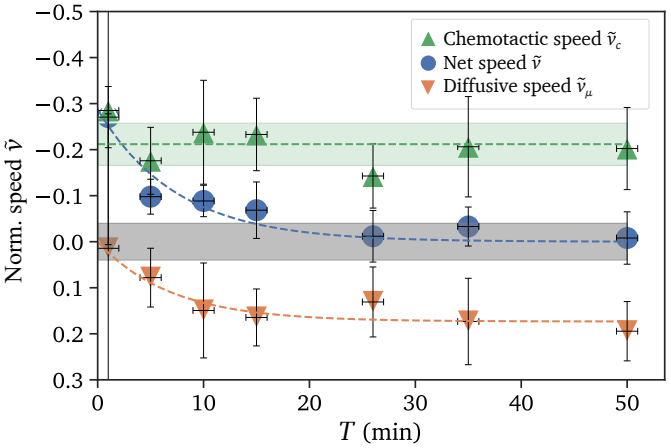

Figure 3: Evolution of the average net, diffusive and chemotactic velocities in a typical experiment measured at $z = h/2$. All velocities are normalised by the swimming speed v_s: blue circles correspond to the net velocity $\tilde{v}$, orange triangles to the diffusive velocity $\tilde{v}_\mu$, and green triangles to the chemotactic velocity $\tilde{v}_c$. The vertical bars indicate the standard deviation of the values on the bands, while the horizontal bars correspond to film acquisition duration. The net and diffusive velocities are fitted by an exponential function $\tilde{v} \propto \exp(-t/\tau^{\text{stat}})$ (dashed lines), with τ^{stat} the characteristic time to reach the stationary state: $\tau^{\text{stat}} \simeq 7\,\text{min}$ for the net velocity, and $\tau_\mu^{\text{stat}} \simeq 9\,\text{min}$ for the diffusive velocity. Green band: average and standard deviation of each average chemotactic velocity value. Grey band: threshold of $\tilde{v}_c$ over which chemotaxis happens. This experiment was performed using MeAsp with $\bar{c} = 100\,\mu\text{M}$ and $\nabla c = 200\,\mu\text{M/mm}$.

In Fig. 3, we have represented the net velocity $\tilde{v}$ and the diffusive velocity $\tilde{v}_\mu$ measured at seven different times for the experiment depicted in Fig. 2. The net velocity is at its highest absolute value at the beginning of an experiment, see blue circles in Fig. 3.

This high negative value indicates that the bacterial population is moving towards the source of the attractant. As time goes on, the absolute net velocity decreases and approaches a value close to zero after 25 min. This decrease is concomitant with an increase in the normalised diffusive velocity $\tilde{v}_\mu$ (orange circles), calculated from the concentration profiles of bacteria as they become more and more uneven. After 25 min, this velocity stabilises to a plateau value as the profile reaches the exponential stationary state (see Fig. 2h). This stationary state is achieved when the diffusive flux is important enough to compensate the chemotactic flux, resulting in a total flux and a net velocity $\tilde{v}$ of zero. As highlighted in Eq. (6), the sum of the net and diffusive velocities at all times T gives the chemotactic velocity $\tilde{v}_c$, see green circles in Fig. 3. The chemotactic velocity is almost constant over time, which is consistent with the existence of a steady linear gradient along the width of the central channel where the bacteria are located, with a mean value close to -0.2 well above the detection threshold (grey band), validating our method.

3.2 Transient and local measurements improve measurement of chemotactic susceptibility

The proposed method, as demonstrated in the previous section, offers an efficient approach to measuring the chemotactic velocity at any point during the experiment. By locally assessing the net velocity and calculating the diffusive velocity based on the bacterial concentration profile, we can determine the chemotactic velocity and, consequently, the chemotactic susceptibility at any given time. This method contrasts with the stationary approach, which only allows for the determination of a single chemotactic velocity from one experiment. We will first focus on the temporal aspect and its dependence on the variable y, while the impact of the height z will be addressed in the following section.

We will first highlight one advantage of our method, which allows us to achieve results faster than the stationary method. The first films of 7 experiments recorded midway between the surfaces, i.e., the films recorded in the early stage of the transient state ($T \leq 3\,\text{min}$), are analysed with the method described in Sec. 2.4. In the early stage of the transient state, the bacterial concentration in the channel remains roughly uniform across the channel width (see Fig. 2h). The diffusive velocity accounts for less than 1 % of the swimming velocity, leading to $v_c \approx v$. Since the chemical gradient across the channel is constant and controlled, the chemotactic susceptibility χ can be determined from Eq. (2). The latter is then plotted as a function of the average chemical concentration in the chan-

nel $\bar{c}$, see blue circles in Fig. 4. The data points obtained from the analysis of the stationary profile are shown as red squares. For both methods, we obtain a clear $1/\bar{c}$ evolution of the chemotactic susceptibility $\chi(\bar{c})$, characteristic of a log-sensing response, over more than three decades. Data collected at all times T can be systematically aggregated to enhance measurement precision. This methodological refinement facilitates a more accurate quantification of the chemotactic response, allowing for improved statistical analysis and greater reliability of the results.

The second strength of the proposed method is the ability to obtain a local measurement of the chemotactic velocity, derived from analysing a specific portion of the entire image. The channel containing the bacteria is divided into bands of width Δy for the analysis. This division allows for a much more precise measurement of the chemotactic response, as the chemotactic velocity calculated in each band can be correlated to the local attractant concentration c instead of the mean concentration $\bar{c} = \langle c \rangle_y$. In each band, we evaluate the chemotactic velocity by analysing the detected trajectories within that band (see Sec. 2.4). Using this analysis, we can calculate the local chemotactic susceptibility, denoted as $\chi(c)$, by applying Eq. (2). Figure 5 presents the calculated values of $\chi(c)$ as a function of the local concentrations of chemoattractants: MeAsp (a) and casamino acids (b). Each blue circle corresponds to one data point, i.e. it is the value of $\chi(y, z = h/2, T)$ for 30 bands at 7 times T and for all n experiments ($n = 24$ for MeAsp, $n = 21$ for casamino acids). A logarithmic binning in c was applied to obtain the larger blue circles with error bars. As in Fig. 4, a clear $1/c$ trend appears over multiple decades in concentration for both chemoattractants. This log-sensing response approximately spans from 1–1×10^4 µM for MeAsp, and from 5×10^2–5×10^5 µM for casamino acids. Outside of these bounds, the chemotactic response seems to deviate from the $1/c$ trend. We, thus, fit our data using Eq. (3), $\chi(c) = \chi_0 / \left((1 + c/c_-)(1 + c/c_+)\right)$, which includes a lower limit (c_-) and an upper limit (c_+) to the log-sensing regime [23, 33, 43, 52]. For both chemicals, the best fit of the data yields the values of both concentration thresholds c_- and c_+ as well as the coefficient χ_0. In practice, those thresholds are found close to the lowest and highest concentration values beyond which the chemotactic velocity becomes lower than the detection threshold determined in Sec. 2.4. For MeAsp, we find $\chi_0 = 2.5 \times 10^3$ µm/µM, $c_- = 5 \times 10^{-2}$ µM and $c_+ = 5 \times 10^4$ µM (see Fig. 5a), while for casamino acids, we find $\chi_0 = 0.7$ µm/µM, $c_- = 2 \times 10^2$ µM and $c_+ = 2 \times 10^5$ µM (see Fig. 5b). The results for MeAsp are consistent with the study by Kalinin *et al.* who found a log-sensing chemotactic response between 5–1×10^4 µM [30]. The chemotactic behaviour in response to a casamino acids gradient also show a similar log-sensing response.

In order to compare our method with the stationary method used in the literature [30, 33, 35], the chemotactic susceptibility derived from the stationary bacterial profile of our experiments is presented as red squares in Fig. 5. The first striking observation is the sheer difference in the quantity of data generated by each method: for the $n = 23$ experiments conducted with a gradient of MeAsp, more than 2×10^5 data points are retrieved with our method compared to only ≈ 80 with the stationary method. Another advantage is the accuracy in the concentration of chemoattractant: as the chemotactic velocity is calculated locally within bands of width Δy, the chemical concentration associated with this chemotactic bias is more accurate than when it is averaged across the whole width of the chamber. Moreover, this also widens the range of concentrations c explored: for MeAsp, significant chemotactic responses are measured from 1 µM to 6×10^3 µM for the mean concentration $\bar{c}$, whereas the range in the local concentration c extends from 5.0×10^{-2}–1.5×10^4 µM.

3.3 Chemotactic drift on surfaces

After quantifying the chemotactic behaviour of *E. coli* in the bulk, we will now focus on its chemotactic response near surfaces, specifically shifting from the analyses in Sections 3.1 and 3.2, which were based on data recorded at a height of $z = h/2$, to films taken on the top and bottom surfaces. As the focal plane depth is roughly 40 µm, bacteria located within $\Delta z \simeq 20$ µm of the surface are detected [35].

At the population level, the behaviour observed on surfaces is consistent with that at $z = h/2$. The bacterial population profile across the channel (see Fig. 2l) transitions from a flat distribution, indicating a homogeneous distribution of bacteria, to one that shows an accumulation of bacteria near the source of the chemoattractant. This pattern mirrors what is observed at $z = h/2$, as shown in Fig. 2h. When examining individual trajectories, we find that bacteria on the surfaces exhibit more circular movement (see Fig. 2i-k) compared to the straighter trajectories observed at $z = h/2$ (see Fig. 2e-g). The presence of circular trajectories on surfaces has been previously documented and can be explained by the hydrodynamic interactions between bacteria and surfaces, which are induced by the rotation of the flagella and the bacterial body [53].

The chemotactic velocities $v_c(y, z, T \leq 3\,\text{min})$ were then evaluated at short times, for all experiments and for the three heights. For these short times $T \leq 3$ min, the chemotactic flux is roughly equal to the net flux as the concentration profile of bacteria is nearly uniform. The distributions

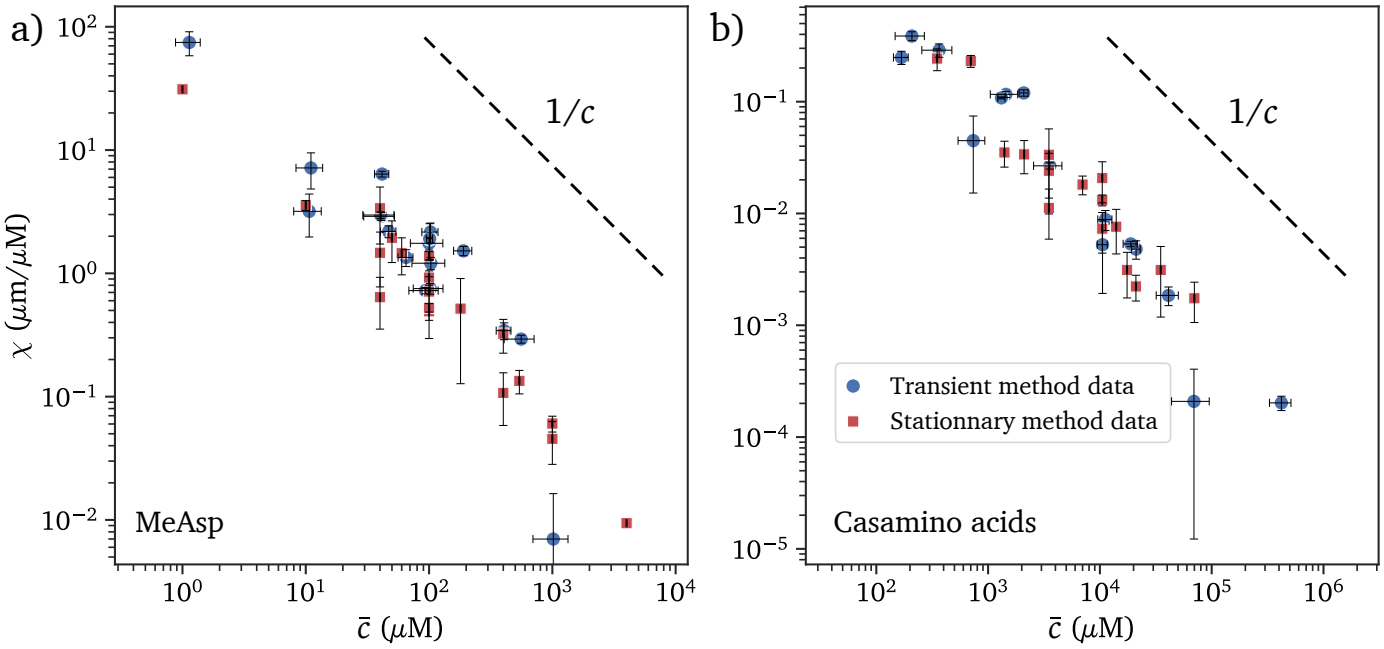

Figure 4: Measuring the bacterial velocity bias in the transient state allows for a much quicker quantification of the chemotactic bias. Chemotactic susceptibility $\chi(\bar{c})$ measured with (a) MeAsp and (b) casamino acids as a function of the average concentration in the channel $\bar{c}$. Blue circles: susceptibility deduced in the transient state ($T \leq 3\,\text{min}$) from the bias in bacterial velocities along the gradient. Red squares: susceptibility deduced from the steady spatial profile of the bacteria [35].

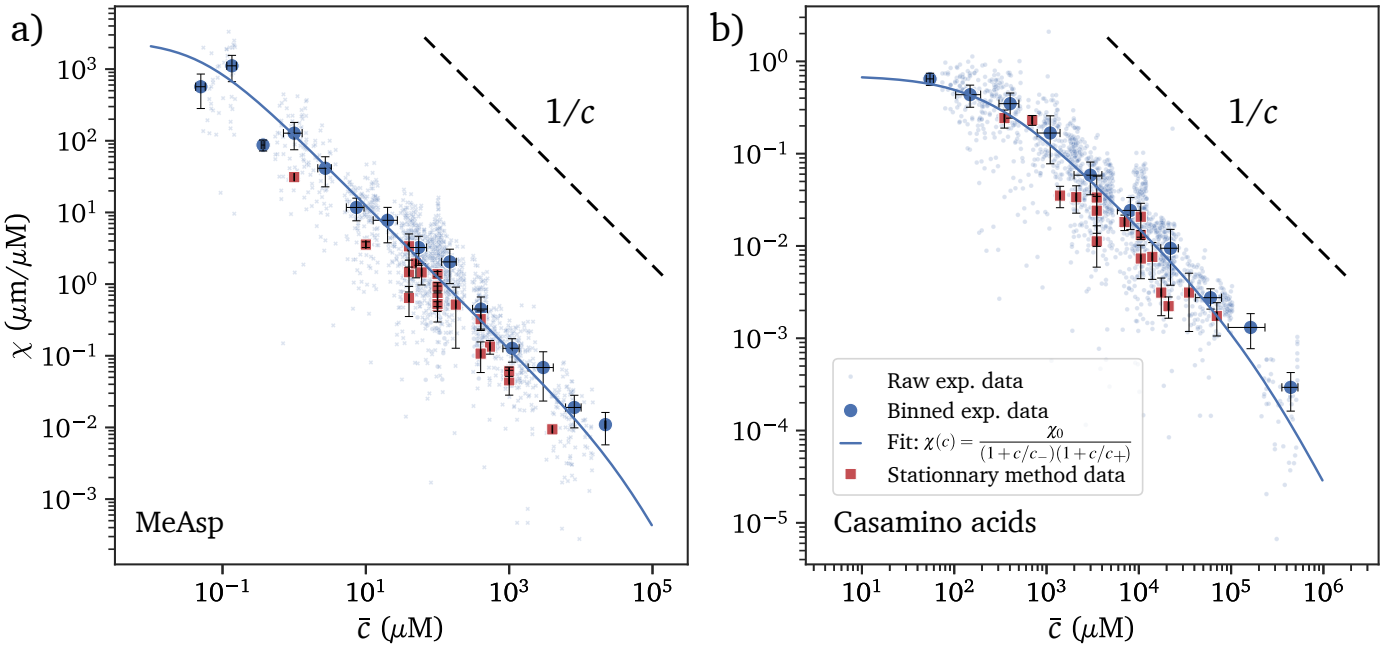

Figure 5: Transient and local measurements allow for a quicker and more accurate quantification of the log-sensing response. Chemotactic susceptibility $\chi(c)$ of chemoattractants (a) MeAsp and (b) casamino acids, respectively, as a function of their local concentration c. Each small shaded blue circle corresponds to the value of the chemotactic susceptibility $\chi(Y,T)$ measured for each band Y of local concentration $c(Y)$ at each time T for each experiment, while the larger blue circles with error bars correspond to their binning in $\log(c)$. Data from the steady spatial profile of the bacteria [35] are shown as ■, one point corresponding to only one experiment. Solid lines: fit of the data as $\chi(c) = \chi_0/((1 + c/c_-)(1 + c/c_+))$, with (a) $\chi_0 = (2.5 \pm 2.0) \times 10^3$ µm/µM, $c_- = (5 \pm 3) \times 10^{-2}$ µM and $c_+ = (5 \pm 3) \times 10^4$ µM for MeAsp, and (b) $\chi_0 = (0.7 \pm 0.4)$ µm/µM, $c_- = (2 \pm 1) \times 10^2$ µM and $c_+ = (2 \pm 1) \times 10^5$ µM for casamino acids. Dashed lines: $\chi(c) \propto 1/c$.

of the normalised net velocities $\tilde{v}(y)$ are thus shown in Fig. 6 at three different heights ($z = 0$, $h/2$ and h). In the experiments conducted without chemical gradients, as illustrated in Fig. 6a, the distributions measured on the surfaces (represented by the blue and green bins) and at mid-height in the cell (represented by the orange bins) overlap significantly. These distributions can be fitted with a Gaussian distribution that has a mean of zero and a root mean square deviation of ≈ 0.05. In the presence of a chemoattractant, and for the measurements taken at $z = h/2$ (shown in orange bins in Fig. 6b and c), the distributions are broader compared to those measured without the attractant and with a negative mean of respectively -0.25 and -0.1. This indicates the chemotactic movement of bacteria towards the source of the chemoattractant, as discussed in the previous sections. The shift and enlargement of the distributions are not observed in the measurements taken on the surfaces (green and blue bins in Fig. 6b and c). The distribution retains the same shape as that measured without a chemoattractant (see Fig. 6a), showing a zero average and a root mean square deviation of ≈ 0.05, clearly suggesting that the surfaces inhibit chemotaxis.

This fascinating effect of surfaces on chemotactic behaviour is consistent with a previous study on *Caulobacter crescentus*' chemotaxis towards MeAsp, which showed a zero net velocity close to surfaces [27].

4 Discussion and Conclusions

Our research presents a novel technique to determine the chemotactic response of bacteria in a chemical gradient. Our approach involves analysing bacterial tracks extracted from films to determine the chemotactic velocity. We assess the total and diffusive velocities to obtain the characteristics of bacterial movement in response to the chemical gradient. We have successfully applied our method to experiments performed in a microfluidic chip where a population of bacteria can be placed in a constant gradient of chemical elements, the 3-channel chip.

By using this method, we assess the chemotactic susceptibility of *E. coli* to MeAsp and casamino acids. The data collected with MeAsp can be compared to existing research [25, 30]. Additionally, the use of casamino acids broadens the approach to include mixed consumable chemoattractants, which are more prevalent in nature. Our measurements are compared with those obtained from analysing the steady-state bacteria concentration profile. We demonstrate that the proposed method is (i) faster, as it does not require waiting for the system to reach a stationary state, which typically takes around twenty minutes; (ii) allows for measurements within a smaller spatial window, facilitating localised analysis of chemotaxis; and (iii) offers improved statistics because more data can be collected during a single experiment. Thanks to these advantages, the concentration range in which a chemotactic response is observed is identified with precision.

For both chemoattractants, the data can be adjusted using Eq. (3), which simplifies to $\chi(c) = \chi_0/c$ when $c_- \ll c \ll c_+$, an evolution consistent with the theoretical analyses of Keller & Segel [38]. According to this scaling law, the chemotactic velocity varies as $\log(c)$, indicating a log-sensing response. This confirms the results previously obtained with MeAsp in a similar microfluidic setup by Kalinin et al [30] and invalidates the scaling law used by Ahmed et al [31]. In the latter case, the difference can be attributed to the narrower concentration range of 0.1–1 mM used compared to our study, which ranges from 0.0001–100 mM. This wider range allows for a more accurate fit of the scaling laws of $\chi(c)$, as well as the determination of the bounds to the log-sensing regime, which could help shed some light on the biochemical processes involved in the detection of chemicals.

Our method was applied to image sequences acquired on surfaces, showing that there is no chemotaxis on the surfaces. We believe this effect can be explained by the shape of the trajectories taken by bacteria near surfaces. Due to hydrodynamic interactions between the bacteria and the surface, their trajectories become circular [53]. This circular motion leads to a reorientation of the swimming direction of the bacteria. Importantly, this reorientation occurs more quickly than the time needed for a chemical signal to provoke a change in the swimming direction of the bacteria in response to variations in chemoattractant concentration. For *E. coli*, tumbling allows the bacteria's body to reorient itself, allowing the bacteria to move away from the surface [54]. As hydrodynamic interaction decreases with distance from the surface, bacteria that move away from the surface experience a reorientation time defined by the run-and-tumble swimming mechanism. This allows for chemotaxis to occur again, enabling the bacteria to migrate toward the source of the chemoattractant. The reorientation mechanism of the bacteria enables them to return to the surface, positioning themselves closer to the source of the chemoattractant this time. This sequence of trapping, escaping, and chemotactic drift results in the distribution of bacteria on the surfaces evolving towards an exponential profile similar to that measured at half-height far from surfaces. This result confirms the inhibitory role of surfaces observed by Grognot and Taute [27] when analysing 3D trajectories of *E. coli* bacteria in a concentration gradient.

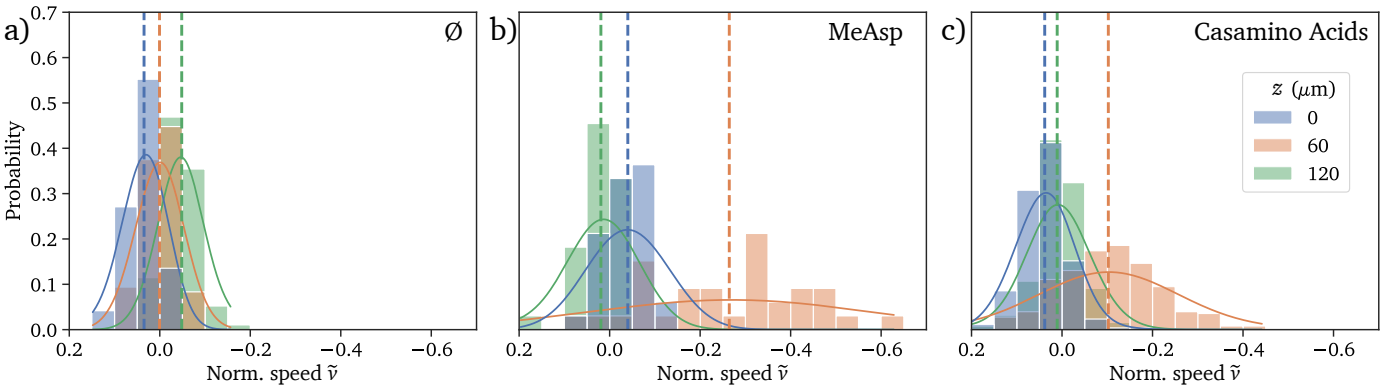

Figure 6: Absence of chemotactic drift on surfaces. Distribution of the normalised net velocity $\tilde{v}(y,T) = v(y,T)/v_s(T)$ for $T \leq 3\,\text{min}$, with (a) no chemo-attractant gradient, (b) a MeAsp gradient of $-0.2\,\mu\text{M}/\mu\text{m}$, and (c) a casamino acids gradient of $-0.7\,\mu\text{M}/\mu\text{m}$. Blue and green histograms show bacteria velocities measured on surfaces, respectively the agar ($z = 0$) and PDMS ($z = h$) surfaces. Orange histograms show the velocity distribution in the bulk at $z = h/2$, halfway between the surfaces. A clear chemotactic drift appears in the bulk when a gradient of chemoattractants is established, while no drift is noticeable on the surfaces. Solid lines: Kernel density plots.

5 Perspectives

One advantage of the method described is that it can be applied to bacteria that respond to chemical gradients differently than *E. coli*. In our method, the velocity v_s and the diffusion coefficient μ are calculated from each image sequence, enabling us to account for these effects. Our approach also allows us to distinguish between different populations of bacteria within the suspension. For instance, we can filter out a subpopulation of non-motile bacteria from the motile ones.

The statistical analysis of bacterial trajectories significantly reduces the experimental time needed to determine chemotactic velocity. We believe that our proposed method will aid in the development of new, faster, and more precise techniques for screening bacterial molecule couples. Finally, the absence of chemotaxis on surfaces opens up interesting perspectives concerning chemotaxis in porous media.

Author Contributions

P.M., H.A. and C.D. conceptualised the research. A.G., J.B., H.A. designed the experiments. J.B. conducted early experiments. A.G. performed the experiments and analysed the data. P.M. and H.A. secured funding. P.M., C.D. and H.A. supervised the project. A.G., J.B. and H.A. wrote the original draft of the manuscript. All authors reviewed the manuscript.

Conflicts of interest

The authors have no conflict to declare.

Acknowledgements

We thank Akash Ganesh and Gaëlle Lextrait for experimental help, as well as Frédéric Moisy for fruitful discussions.

This work is supported by the French National Research Agency (ANR) through the "Laboratoire d'Excellence Physics Atom Light Mater" (LabEx PALM) as part of the "Investissements d'Avenir" program (ANR-10-LABX-0039), and by the CNRS through the Mission for Transversal and Interdisciplinary Initiatives (MITI), part of the 80 Prime program (RootBac project).

References

[1] H. C. Berg, *Annual Review of Biophysics and Bioengineering*, 1975, **4**, 119–136.

[2] J. Adler, *Annual Review of Biochemistry*, 1975, **44**, 341–356.

[3] R. Karmakar, *Journal of Basic Microbiology*, 2021, **61**, 366–379.

[4] J.-B. Raina, B. S. Lambert, D. H. Parks, C. Rinke, N. Siboni, A. Bramucci, M. Ostrowski, B. Signal, A. Lutz, H. Mendis, F. Rubino, V. I. Fernandez, R. Stocker, P. Hugenholtz, G. W. Tyson and J. R. Seymour, *Nature*, 2022, **605**, 132–138.

[5] J.-B. Raina, V. Fernandez, B. Lambert, R. Stocker and J. R. Seymour, *Nature Reviews Microbiology*, 2019, **17**, 284–294.

[6] H.-H. Tsai, Y. Tang, L. Jiang, X. Xu, V. D. Tendon, J. Pang, Y. Jia, K. Wippel, J. Vacheron, C. Keel, T. G. Andersen, N. Geldner and F. Zhou, *Science*, 2025, **390**, eadu4235.

[7] G. Lextrait, S. Joardar, R. Cossard, Y. Kikuchi, T. Ohbayashi and P. Mergaert, *ISME Journal*, 2025, **in press**,.

[8] P. M. Merritt, T. Danhorn and C. Fuqua, *Journal of Bacteriology*, 2007, **189**, 8005–8014.

[9] J. Armitano, V. Méjean and C. Jourlin-Castelli, *Environmental Microbiology*, 2013, **15**, 3108–3118.

[10] L. Stricker, I. Guido, T. Breithaupt, M. G. Mazza and J. Vollmer, *Journal of The Royal Society Interface*, 2020, **17**, 20200559.

[11] J. M. Keegstra, F. Carrara and R. Stocker, *Nature Reviews Microbiology*, 2022, **20**, 491–504.

[12] R. M. Ford and R. W. Harvey, *Advances in Water Resources*, 2007, **30**, 1608–1617.

[13] B. Bhushan, S. K. Samanta, A. Chauhan, A. K. Chakraborti and R. K. Jain, *Biochemical and Biophysical Research Communications*, 2000, **275**, 129–133.

[14] D. Paul, R. Singh and R. K. Jain, *Environmental Microbiology*, 2006, **8**, 1797–1804.

[15] H. Harms and L. Wick, *Engineering in Life Sciences*, 2006, **6**, 252–260.

[16] K. Yamamoto-Tamura, I. Kawagishi, N. Ogawa and T. Fujii, *Bioscience, Biotechnology, and Biochemistry*, 2015, **79**, 926–936.

[17] J. Adler, *Journal of General Microbiology*, 1973, **74**, 77–91.

[18] F. Dahlquist, P. Lovely and D. Koshland, *Nature New Biology*, 1972, **236**, 120–123.

[19] M. Holz and S. Chen, *Biophysical Journal*, 1978, **23**, 15–31.

[20] R. M. Ford, B. R. Phillips, J. A. Quinn and D. A. Lauffenburger, *Biotechnology and Bioengineering*, 1991, **37**, 647–660.

[21] P. Lewus and R. M. Ford, *Biotechnology and Bioengineering*, 2001, **75**, 292–304.

[22] N. Morales-Soto, M. E. Anyan, A. E. Mattingly, C. S. Madukoma, C. W. Harvey, M. Alber, É. Déziel, D. B. Kearns and J. D. Shrout, *Journal of visualized experiments: JoVE*, 2015, e52338.

[23] J. Cremer, T. Honda, Y. Tang, J. Wong-Ng, M. Vergassola and T. Hwa, *Nature*, 2019, **575**, 658–663.

[24] S. Kim, H. J. Kim and N. L. Jeon, *Integrative Biology*, 2010, **2**, 584.

[25] T. Ahmed, T. S. Shimizu and R. Stocker, *Integrative Biology*, 2010, **2**, 604.

[26] J. Wu, X. Wu and F. Lin, *Lab on a Chip*, 2013, **13**, 2484.

[27] M. Grognot and K. M. Taute, *Communications Biology*, 2021, **4**, 669.

[28] J. Diao, L. Young, S. Kim, E. A. Fogarty, S. M. Heilman, P. Zhou, M. L. Shuler, M. Wu and M. P. DeLisa, *Lab on a Chip*, 2006, **6**, 381–388.

[29] S.-Y. Cheng, S. Heilman, M. Wasserman, S. Archer, M. L. Shuler and M. Wu, *Lab on a Chip*, 2007, **7**, 763.

[30] Y. V. Kalinin, L. Jiang, Y. Tu and M. Wu, *Biophysical Journal*, 2009, **96**, 2439–2448.

[31] T. Ahmed, T. S. Shimizu and R. Stocker, *Nano Letters*, 2010, **10**, 3379–3385.

[32] K. Son, F. Menolascina and R. Stocker, *Proceedings of the National Academy of Sciences*, 2016, **113**, 8624–8629.

[33] F. Menolascina, R. Rusconi, V. I. Fernandez, S. Smriga, Z. Aminzare, E. D. Sontag and R. Stocker, *npj Systems Biology and Applications*, 2017, **3**, 16036.

[34] M. Morse, R. Colin, L. G. Wilson and J. X. Tang, *Biophysical journal*, 2016, **110**, 2076–2084.

[35] A. Gargasson, C. Douarche, P. Mergaert and H. Auradou, *Bio-protocol*, 2025, **15**, e55184.

[36] E. F. Keller and L. A. Segel, *Journal of theoretical biology*, 1971, **30**, 225–234.

[37] M. A. Rivero, R. T. Tranquillo, H. M. Buettner and D. A. Lauffenburger, *Chemical Engineering Science*, 1989, **44**, 2881–2897.

[38] L. A. Segel, *SIAM Journal on Applied Mathematics*, 1977, **32**, 653–665.

[39] E. F. Keller and L. A. Segel, *Journal of Theoretical Biology*, 1971, **30**, 235–248.

[40] G. L. Hazelbauer, J. J. Falke and J. S. Parkinson, *Trends in Biochemical Sciences*, 2008, **33**, 9–19.

[41] L. Laganenka, R. Colin and V. Sourjik, *Nature Communications*, 2016, **7**, 12984.

[42] Y. Tu, T. S. Shimizu and H. C. Berg, *Proceedings of the National Academy of Sciences*, 2008, **105**, 14855–14860.

[43] G. Si, T. Wu, Q. Ouyang and Y. Tu, *Physical Review Letters*, 2012, **109**, 048101.

[44] R. Colin, R. Zhang and L. G. Wilson, *Journal of The Royal Society Interface*, 2014, **11**, 20140486.

[45] S. I. Bibikov, A. C. Miller, K. K. Gosink and J. S. Parkinson, *Journal of Bacteriology*, 2004, **186**, 3730–3737.

[46] L. Stricker, I. Guido, T. Breithaupt, M. G. Mazza and J. Vollmer, *Journal of The Royal Society Interface*, 2020, **17**, 20200559.

[47] J. Bouvard, C. Douarche, P. Mergaert, H. Auradou and F. Moisy, *Physical Review E*, 2022, **106**, 034404.

[48] J.-Y. Tinevez, N. Perry, J. Schindelin, G. M. Hoopes, G. D. Reynolds, E. Laplantine, S. Y. Bednarek, S. L. Shorte and K. W. Eliceiri, *Methods*, 2017, **115**, 80–90.

[49] P. S. Lovely and F. Dahlquist, *Journal of theoretical biology*, 1975, **50**, 477–496.

[50] J. Taktikos, H. Stark and V. Zaburdaev, *PloS one*, 2013, **8**, e81936.

[51] E. Lauga, *The Fluid Dynamics of Cell Motility*, Cambridge University Press, 2020.

[52] R. Alert, A. Martínez-Calvo and S. S. Datta, *Physical Review Letters*, 2022, **128**, 148101.

[53] E. Lauga and T. R. Powers, *Reports on progress in physics*, 2009, **72**, 096601.

[54] G. Junot, T. Darnige, A. Lindner, V. A. Martinez, J. Arlt, A. Dawson, W. C. Poon, H. Auradou and E. Clément, *Physical Review Letters*, 2022, **128**, 248101.

[55] A. Ganesh, *Theses*, Université Paris-Saclay, 2023.

[56] A. Gargasson, *Theses*, Université Paris-Saclay, 2025.

Supplementary Material

A Effect of the chemoattractant concentration and gradient on the swimming velocity and motility

The influence of chemoattractants on bacterial motility was investigated. Each film was analysed to determine the swimming velocity of the bacteria v_s and the decorrelation time of the trajectories τ. The same analysis was carried out on the experiments without chemoattractants to determine the influence of chemical species on bacterial motility. Figures 7 and 8 show the relevant quantity, v_s and τ respectively, averaged over all seven times T in an experiment. The vertical bars represent the quadratic deviation of the data measured. In the figures, the values obtained for the experiments conducted without a chemoattractant are shown with a dotted line and a grey background. Each symbol denotes a unique batch of bacteria, making measurement variations likely due to differences between batches.

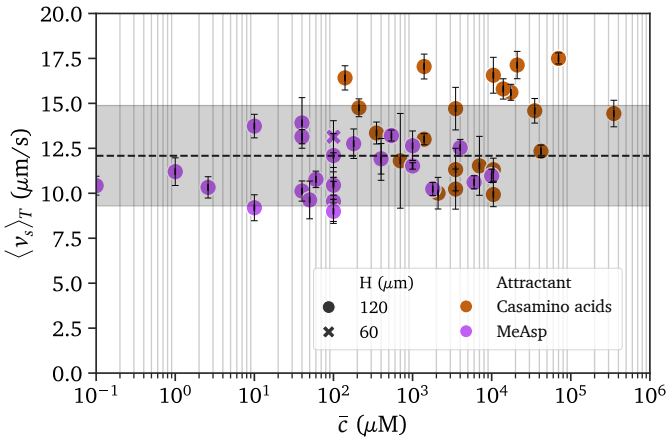

Figure 7: Bacterial swimming velocity $\langle \bar{v}_s \rangle_T$ as a function of chemoattractant concentration. Purple and orange markers correspond respectively to α-methyl-DL-aspartic (MeAsp) and casamino acids. The average is done over all the image sequences recorded during one experiment. Horizontal dashed line: average velocity for three experiments without chemoattractant ($c_1 = c_3 = 0$). The grey zone indicates the range of variation of v_s in the absence of a gradient. Vertical bars: second moment of the distribution of the velocities.

Table 1 gives the values of the swimming velocity and decorrelation time averaged over all the experiments performed with or without attractants. The diffusion coefficients μ derived from the equation $\mu = v_s^2 \tau$ are consistent with the range reported in the literature (see for example, Tab. 2 in [21] or [31]).

Solute	v_s (μm/s)	τ (s)	μ (μm^2/s)
ø	11 ± 2	1.7 ± 0.7	200 ± 80
Cas. acids	13 ± 2	1.3 ± 0.6	210 ± 100
MeAsp	11 ± 1	2.0 ± 0.4	250 ± 70

Table 1: Swimming velocity v_s, correlation time τ and diffusion coefficient μ in absence of chemo attractant (ø), with casamino acids (Cas. acids) and α-methyl-DL-aspartic (MeAsp). The values are the averages of all the films taken at half-height in the channel.

B Verification of the shallow gradient assumption

A series of experiments was conducted to verify the shallow gradient limit in our studies and to validate the use of Eq. (2). To achieve this, the values of c_1 and c_3 were adjusted so that the average concentration $\bar{c}$ remained constant, while the gradient varied. Fig. 9 shows the normalised averaged chemotactic velocity $\tilde{v}_c$ as a function of the imposed gradient. The data points align on a straight line with a slope of $\chi(\bar{c}) = 0.75\,\mu\text{m}/\mu\text{M}$. Based on this result, we see that the chemotactic susceptibility can be obtained from the measurement of v_c knowing the imposed gradient ∇c as: $\chi(\bar{c}) = v_c/\nabla c$.

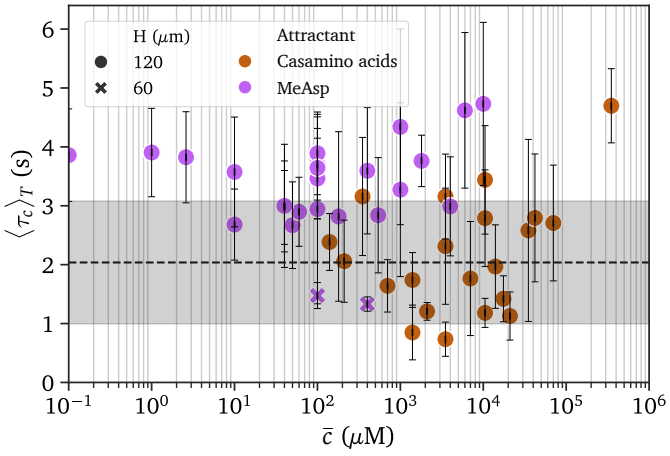

Figure 8: Average correlation time $\langle \tau \rangle_T$ estimated from the velocity correlation function. Purple and orange markers correspond respectively to MeAsp and casamino acids. The average is done over all the image sequences recorded during one experiment. Horizontal dashed line: correlation time averaged over three experiments performed without casamino acids in the reservoir channels ($c_1 = c_3 = 0\,\text{mM}$). Grey zone: the range of variation of the correlation time without a gradient. Vertical bars indicate the second moment of the correlation time distribution.

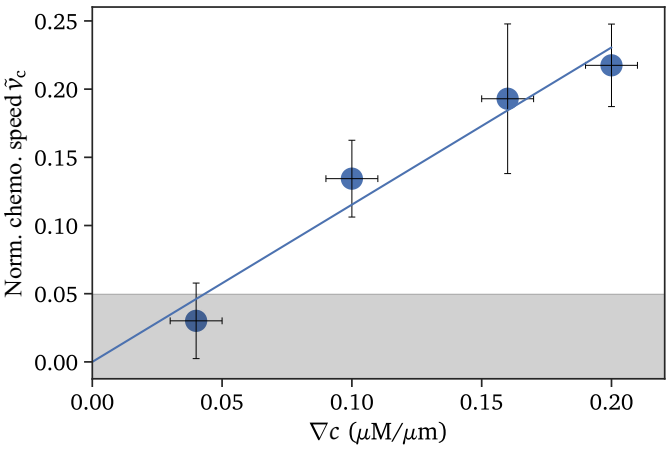

Figure 9: Normalised chemotactic velocity $\langle \tilde{v}_c(T) \rangle_T$, averaged over all times T, as function of ∇c measured for an average MeAsp concentration of $\bar{c} = 100\,\mu\text{M}$. The solid line is a linear fit of the data by $\tilde{v}_c = \chi \nabla c$ with $\chi = (0.72 \pm 0.05)\,\mu\text{m}/\mu\text{M}$. The vertical bars represent the second moment of the distribution of $\tilde{v}_c(T)$.

C Verification of the steady-state of casamino acids' gradient

Unlike MeAsp, casamino acids can be metabolised by *E. coli*. To maintain a stable concentration of casamino acids, it is essential to ensure that their consumption by the bacteria does not exceed the rate at which they are replenished by diffusion from the lateral channels.

Casamino acids are relatively small molecules with a diffusion coefficient $D_{\text{CA}} \approx 400\,\mu\text{m}^2/\text{s}$. To diffuse over a distance $L = 1000\,\mu\text{m}$, equivalent to the distance between channels ① and ③ (see Fig. 1), it requires approximately $T_D = L^2/D_{\text{CA}} \approx 2.5 \times 10^3\,\text{s}$. At the same time, casamino acids are consumed at a rate below $0.05\,\mu\text{M}/(\text{OD}\,\text{s})$ [55]. In our experiments, OD ≈ 0.08, and $\bar{c} < 3 \times 10^5\,\mu\text{M}$. Hence, the characteristic consumption time is $7.5 \times 10^7\,\text{s} \gg T_D$. The time taken for consumption is significantly longer than that for diffusion; therefore, the metabolisation of the attractant can be disregarded. The conservation equation for both chemoattractants, MeAsp and casamino acids, can thus be written as follows:

$$\partial_t c = -D \partial_y^2 c \tag{9}$$

with D the diffusion coefficient of the chemoattractant and c its concentration [56]. In the steady state ($\partial_t c \sim 0$) with constant concentrations in channels ① and ③, the concentration varies with a constant gradient given by $\nabla c = (c_1 - c_3)/L$.